# Numerical Study of the Wetting Dynamics of Surfaces Textured by Femtosecond Laser: Beyond Classical Wenzel and Cassie-Baxter Model

Ilemona S. Omeje[a], Tatiana E. Itina[a]

[a]*Laboratoire Hubert Curien, UMR CNRS 5516, Université Jean Monnet, Universite de Lyon, Saint-Etienne, France*
*Corresponding author: ilemona.sunday.omeje@univ-st-etienne.fr*

## Abstract

The classical wetting models, such as the Wenzel and Cassie-Baxter have been extensively used to quantify laser textured surfaces. However, these models do not provide enough explanations for wettability of femtosecond textured surfaces. In this work, we propose a continuum-level modelling to study the wetting dynamics of a water droplet on Ti-6Al-4V alloy. The calculations are performed for plain solid surfaces and surfaces with various reliefs. The calculated evolutions of the spreading parameter for both structured and non-structured surfaces not only provide explanations of several experimental results, but also underline the perspectives of using hierarchical reliefs for efficient wettability control. Thus, such simulations are shown to be useful in the relief design and laser texturing for a wide range of applications.

*Keywords:* Femtosecond Laser, Wettability, Spreading Parameter, Equilibrium Contact Angle, Surface Relief

## 1. Introduction

It is well-known that laser pulses interacting with solid surfaces often create a set of periodic or non-periodic surface structures ranging from "ripples" also known as laser-induced periodic surface structures (LIPSS) to grooves and spikes. Additionally, when laser scanning systems are used, so-called hierarchical structures can be easily formed on surfaces combining both micro- and nano-reliefs and allowing a wide-range control over surface wettability [1][2][3]. One of the promising applications of such effects is in the integration and durability of dental and orthopedic implants [4][5]. Other modern applications include self-cleaning glasses and microfluidic in-jet printing [6][7]. When femtosecond lasers are used, the control possibilities are considerably enhanced. Depending on laser parameters, femtosecond textured designed surfaces can be either high-spatial frequency or low-frequency LIPPSS with various orientations, cones, pillars, as well as various combinations of these structures that can be obtained by using additional optical filters and polarization devices, laser beam interferomentry set-ups, double-pulse irradiation, etc. [8]. The wettability of laser textured surfaces changes not only as a function of surface relief, but also with time [3][9]. The reasons for these changes are currently under investigations. Several time-scales have been

revealed, the shorter one being related to the droplet evolution upon its interaction with the surface, while the longer one is often related with the changes in surface chemistry due to oxydation, molecular adsorption, etc. Extensive experimental work has been performed to examine the influence of femtosecond textured designed surfaces on wettability to improve implant condition. For example, Cunha et. al. [9] reported that biomedical grade titanium-6aluminum-4vanadium (Ti-6Al-4V) alloy surfaces textured by femtosecond laser possesses anisotropic wetting. While Klos et. al. [10] recently reported that laser-induced topographies on Ti-6Al-4V alloy influenced surface wettability and protein adsorption with promotion of osteogenic differentiation.

The wettability of an ideal homogeneous and smooth surface is commonly described by the classical Young's law [11] that balances the three interfacial forces at the contact-line of solid-vapor, solid-liquid and liquid-vapor. The Young's equation can predict the intrinsic equilibrium contact angle (CA), which relates on the surface tension between the three-phases. In reality, surface roughness is an important parameter controlling the contact angle and hence, the wettability [12][13]. Wenzel [13] and Cassie-Baxter [14] proposed modified theoretical models to correct the Young's equation by accounting for surface roughness and the presence of air entrapped on textured surfaces. In the past decades, advancing and receding contact angle in experimental observations has always been replaced with equilibrium contact angle in the corrected models to interpret the behavior of liquid on rough surfaces. Furthermore, Wenzel model predicts that roughness enhances the intrinsic wetting behavior of a surface with the assumption that liquid fully penetrates the solid roughness with a roughness factor. Wenzel argument was partially validated experimentally by Onda et. al. [15] and Shibuichi et. al. [16]. However, Onda et. al. [15] revealed the limitations of Wenzel model for extremely rough surfaces. On the other hand, Cassie-Baxter model [14] assumed that, on such surface, a large fraction of air is entrapped, and the liquid do not completely penetrate the textured surface. Invasion of the liquid on the textured surface takes place through capillary phenomenon, while the remaining liquid sits on the surface [17]. Quere [18] and Bico et. al. [19] attempted to combine the two models to explain the effect of roughness on wetting state. In addition, there are several arguments on whether Wenzel and Cassie-Baxter model can accurately predict some of the experimental trend for textured surfaces including femtosecond textured materials. In fact, McHale [20] reported that Wenzel and Cassie-Baxter equations can be applied only (a) when the surface is similar and isotropic and (b) when the size ratio to the roughness is large enough. In most cases, these models are often oversimplified for wetting studies of laser textured surfaces. The development of much more realistic models is challenging, but it is required for better relief design, namely in many modern laser applications.

Several numerical models have been proposed and deployed to study the wettability of a surface, wetting interaction at the three-phase – solid-liquid-vapor interface – and droplet spreading mechanism. For example, Sikalo et.al. [21] used the Volume of Fluid (VOF) method to study the effect of droplet on flat surface. Meanwhile, Grewal et. al. [22] used the Level Set Method (LSM) to show that topography along with the surface chemistry and geometrical parameters control the wetting performance of patterned surfaces. Chamakos et. al. [23] tried to tackle the contact-line boundary condition of spreading dynamics on textured substrates by using the continuum-level approach. Also, Yagub et. al. [24] used Shan and Chen (SC) lattice Boltzmann model (LBM) [25] to highlight the strength and weaknesses of

the SC model in the description of changes in the droplet apparent contact angle observed on nano/micro structured surfaces. Despite an enormous interest and a high number of studies, many questions have not been enough addressed yet. For instance, the effects of hierarchical surface reliefs were not sufficiently studied theoretically. There is still a lack of understanding of the dynamics of liquid droplets on such surfaces.

In this work, we use a continuum-level modelling method such as LSM to study the wetting dynamics of a water droplet on Ti-6Al-4V alloy. The wetting studies are performed on both plain solid surfaces and on surfaces with hierarchical and periodic triangular reliefs. The spreading parameter (or diameter) of the droplet as a function of the contact time is utilized to examine the short-scale droplet dynamics on several textured materials. In particular, we pay attention to the effects of surface reliefs, velocity and viscosity of droplet evolution on Ti-6Al-4V alloy surfaces.

## 2. Modeling details

Firstly, we started by developing a model of a two-phase flow on a solid surface. For simplicity, the following assumptions have been made. (a) Two immiscible fluids, air and liquid (e.g. water), on plane (and relief) surfaces are assumed to be Newtonian, incompressible and laminar. (b) The droplet-wall collision is considered to be isothermal i.e., both the fluid and the surface are at constant temperature and (c) no heat transfer is considered during the interaction between the wall and the liquid (i.e. adiabatic case). The two-phase flow dynamic is simulated by using the time-dependent in-compressible Navier-Stokes and continuity equations for conservation of mass and momentum as shown in eqs. 1 and 2.

$$\rho(\frac{\partial u}{\partial t} + (u.\nabla)u) = \nabla.[-pI + \mu(\nabla u + (\nabla u)^T) + \rho.g + F_{s_t}] \tag{1}$$

$$\rho\nabla.u = 0 \tag{2}$$

Here $\rho$ and u are the fluid density $(kg/m^3)$ and velocity vector (m/s); p denotes the pressure, I is the second order identity matrix, $\mu$ represents the dynamic viscosity, g is the gravitational acceleration $(m/s^2)$ and represents the surface tension force (N/m). The surface tension force is calculated as follows.

$$F = \nabla T = \nabla.[(\sigma(I - nn^T))\delta] \tag{3}$$

I is the identity matrix, $n$ is the normal to the interface, $\sigma$ is the surface tension and $\delta$ is Dirac delta function that is nonzero only at the fluid interface. Because the two fluids are immiscible, the conservative level set method (LSM) proposed by Olsson and Kreiss [26] is used to track the fluid interface. The interface is captured by level-set function represented by a smeared Heaviside function ($\phi$). $\phi$ changes smoothly across the interface from 0 (in air) to 1 (in liquid) and the interface is represented by $\phi = 0.5$. The LSM eqs. is shown in eqs. (4).

$$\frac{\partial \phi}{\partial t} + u.\nabla\phi = \gamma\nabla.(\varepsilon_l\nabla\phi - \phi(1 - \phi)\frac{\nabla\phi}{|\nabla\phi|}) \tag{4}$$

Here, $\varepsilon_l$ and $\gamma$ represents the artificial thickness of the interface and the re-initialization parameter of the level set function. $\varepsilon_l$ value is taken has half of the mesh size and $\gamma$ value

is defined as the initial value of impact velocity of droplet. The right and left-hand side of eqs. 4 are necessary for numerical stability and movement of the interface. Both $\rho$ and $\mu$ are functions of $\phi$ as shown in eqs. 5 and 6, and are considered to vary smoothly over the interface.

$$\rho = \rho_1 + (\rho_2 + \rho_1)\phi \tag{5}$$

$$\mu = \mu_1 + (\mu_2 + \mu_1)\phi \tag{6}$$

Here, $\rho_1$, $\rho_2$, $\mu_1$ and $\mu_2$ are the densities and dynamic viscosities (Pas) of air and water. Eqs. 1 to 6 are computed by using the finite-element solver discretized in COMSOL Multiphysics 5.6 software [27]. The simulation is performed in 2D axis-symmetry (Fig. 1) to safe computational cost. Open boundary condition was imposed on all the boundary with zero pressure except for the wetted wall. In addition, equilibrium contact angle (ECA) was utilized as the solid boundary condition at the triple contact-line for the setting of the surface wettability instead of static contact angle. This enables us to capture the experimental trend of wettability of femtosecond textured materials. The ECA is estimated from the advancing ($\theta_{adv}$) and receding CA ($\theta_{rec}$) using the theoretical work of Tadmor [28] as shown in eqs. 7, 8 and 9.

$$\theta_{ECA} = cos^{-1}\left(\frac{r_{adv}cos(\theta_{adv}) + r_{rec}cos(\theta_{rec})}{r_{adv} + r_{rec}}\right) \tag{7}$$

where,

$$r_{adv} = \left(\frac{sin^3(\theta_{adv})}{2 - 3cos(\theta_{adv}) + cos^3(\theta_{adv})}\right) \tag{8}$$

and,

$$r_{rec} = \left(\frac{sin^3(\theta_{rec})}{2 - 3cos(\theta_{rec}) + cos^3(\theta_{rec})}\right) \tag{9}$$

Navier slip boundary condition is adopted for the wetted wall and the contact angle to avoid singularity. Thus, a frictional force ($F_{fr} = \mu_\phi u/\beta$) is added, where $\beta$ is the slip length, which is taken as half of the grid size [27] and $u$ is the slip length velocity.
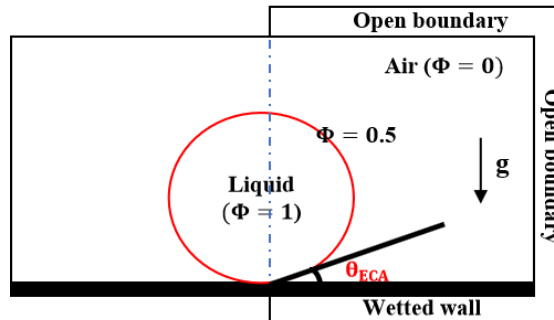


Figure 1: 2D axis-symmetry simulation domain.

## 2.1. Model validation

To check the validity of model described above, we performed the simulation of water droplet impact on hydrophobic surfaces and compared the results obtained with the experimental results of Lin et. al. [29] and Yokoi et.al. [30]. The model was then adopted for different periodic triangular and hierarchical Ti-6Al-4V alloy relief surfaces in order to elucidate the optimum relief required to understand the wetting dynamics of femtosecond textured materials for biomedical application.

Table 1: Estimated equilibrium contact angle

| Type of plane surface | Advancing CA ($\theta_{adv}$) | Receding CA ($\theta_{rec}$) | Estimated $\theta_{ECA}$ [28] |
|---|---|---|---|
| N-BK7 glass | $111^o$ | $100^o$ | $106^o$ |
| Wax | $105^o$ | $75^o$ | $90^o$ |

The first case of the validation was performed by using the experimental data of Lin et. al. [29]. The diameter of water droplet ($D_o$) on N-BK7 glass is 2 mm with an initial impact velocity ($u_o$) of of 0.52 m/s and dynamic viscosity ($\mu_2$) of 0.9 mPas at a surface tension of 71.8 mN/m. The density of droplet is 997 $kg/m^3$ and the estimated ECA used in the simulation is $106^o$ as shown in Table 1. The results of the 2D and 3D time-lapsed images of water droplet impact on the N-BK7 glass surface and those of the current study are presented in Fig. 2. There is an excellent agreement between the experimental results of Lin et. al. [29] and our numerical simulation. Before the impact, the droplet shape is spherical, the droplet deforms and spreads rapidly on the surface. It starts to recoil at 3ms. In fact, at 7.25ms, an entrapped bubbled is observed. This effect is known to be due to the fast rate of recoiling and a capillary wave formation [21][31].
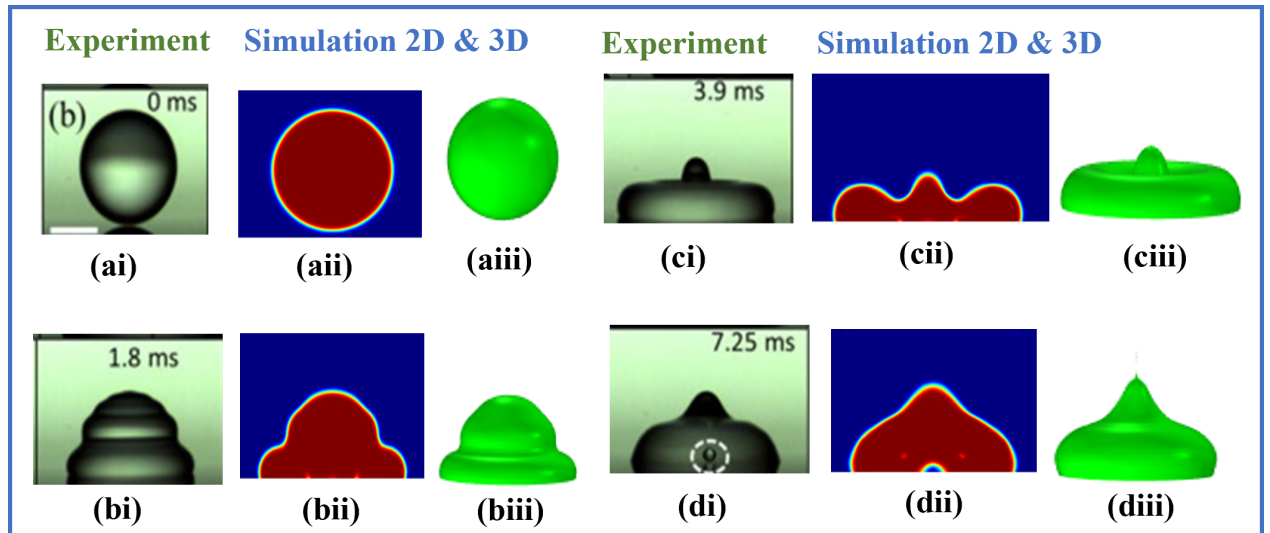


Figure 2: Comparison of experimental data of [29] with 2D and 3D droplet of the current study at 0, 1.8, 3.9 and 7.25 ms respectively.

The second model validation was carried out by using the experimental study of Yokoi et.al. [30]. The initial water droplet diameter ($D_o$) is 2.28 mm with the impact velocity
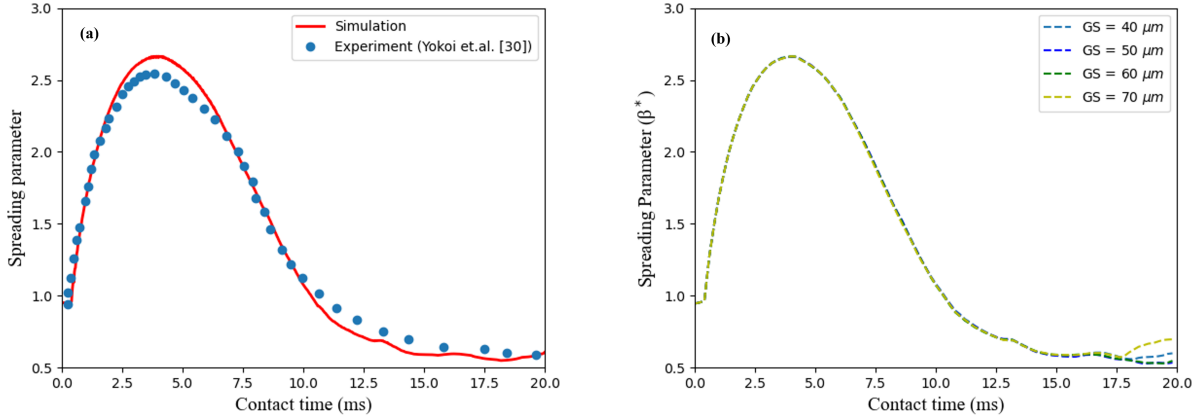
Figure 3: (a) Spreading parameter of water on wax surface (b) Grid convergence test.

$(u_o)$ of 1m/s at estimated ECA of $90^o$. The surface tension is 7.2 mN/m, dynamic viscosity and density of droplet are 1 mPas and 1000 $kg/m^3$. The plot of the spreading parameter $(\beta^*)$ of water droplet on wax surface is compared with the experimental findings [30]. It should be noted that the spreading parameter $(\beta^*)$ is calculated by normalizing the droplet diameter (d) obtained as a function of the contact time by the initial droplet diameter $(D_o)$. As presented in Fig. 3(a), the calculated $(\beta^*)$ agrees well with the experimental values. Moreover, during both the impact and the recoil of the water droplet on wax, an excellent agreement is observed. However, small deviation can be noticed at the peak of the $\beta^*$. This deviation is probably due to the differences observed in the receding contact angle during experiment. The experimental study of Yokoi et.al. [30] utilizes the dynamics contact angle to estimate an appropriate ECA, which makes it suitable for the current study.

Before the simulation of water droplet on different Ti-6Al-4V relief surfaces, we performed a grid sensitivity test of water droplet on wax surface to see where the numerical simulation result converges. For this, different grid sizes (GS) from 40 $\mu m$ to 70 $\mu m$ with a step size of 1mm was used to calculate $\beta^*$ as presented in Fig. 3(b). It is observed that the simulation results of $\beta^*$ converges at a grid size of of 40 $\mu m$ to 60 $\mu m$ with little deviation at 70 $\mu m$. We, therefore, maintained the grid size of 40 $\mu m$ throughout this study. Again, the results of the numerical model and the experimental results match. It is also worth noting that the liquid droplet is sensitive to the type of substrate surface used in the computation [32]. So, the model predicts accurately enough the droplet interaction and spreading on several surfaces.

## 3. Result and discussion

### 3.1. Effects of surface reliefs on wettability of several textured Ti-6Al-4V surfaces

It has been established experimentally that surface roughness influences wetting properties of structured Ti-6Al-4V alloy [3][4]. Interestingly, femtosecond textured Ti-6Al-4V alloy is hydrophilic upon texturing and becomes superhydrophobic with time [3][9]. Nonetheless, we considered periodic triangular and hierarchical surfaces reliefs on Ti-6Al-4V alloy to mimic, at the first approximation, the typical LIPSS of femtosecond textured material [33].

Previously, a series of wetting tests were performed to explain the effect of these reliefs on wettability of the femtosecond laser textured Ti-6Al-4V alloy and to correlate it with HSCs stem cell behavior [10] for better understanding of osseointegration process. To simulate the related process, the area fractions ($\phi_s = 1/2(\text{pq})$) of the plan surface, triangular or hierarchical one, that are assumed to be covered by the liquid droplet is expected to be 0 $\mu m^2$, 0.375 $\mu m^2$ and 1.1 $\mu m^2$ respectively. Here, p is the height and q is the width of the structure. A typical representation of these reliefs are presented in Fig. 4(a) and 4(b).
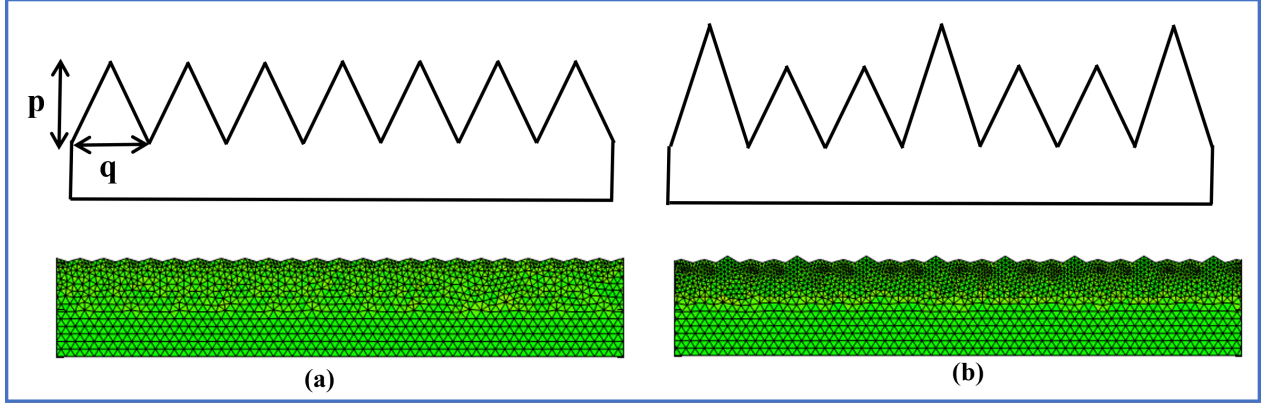


**(a)**                                                                 **(b)**

Figure 4: (a) Periodic triangular and (b) hierarchical surface reliefs used in our simulations.

The diameter ($D_o$) of water droplet is 2.35mm with an impact velocity ($u_o$) of 1m/s at an equilibrium contact angle ($\theta_{ECA}$) of $96^o$ which correspond to the $\theta_{ECA}$ of Ti-6Al-4V alloy after laser texturing [9][10]. The Reynolds number, Re = $\rho u_o D_o/\mu$ is 2345.3 and Weber number, We = $\rho u^2 D_o/\sigma_{la}$ is 32.216. Where $\rho$ is 998 kg/m³, $\sigma_{la}$ is 72.8 mN/m and $\mu$ is 1 mPas. The deformation of water droplet on solid, triangular and hierarchical Ti-6Al-4V relief are shown in Fig. 6 (a),(b) and (c). The calculated spreading diameter ($\beta^*$) and droplet thickness ($\alpha^* = h/D_o$) of water droplet on Ti-6Al-4V relief surfaces are illustrated in Fig. 5 (a) and (b). Here, h is the droplet height. The hydrodynamic of the droplet upon impact on solid Ti-6Al-4V, Fig. 6(a), is controlled by inertial and impact pressure, and the droplet deforms and start to spread rapidly at 8 $\mu s$ to reach a $\beta^*$ of 2.60mm at 4ms. A raised rim is formed at the periphery at 5.6 ms due to surface tension [32] and it starts to retract at 6.6 ms. At 9 ms, the droplet rebounds with an entrapped bubbled. As was discussed before, the bubble is formed due to the fast rate of recoiling and the capillary force. In this study, the rebounding is neglected as we are only concerned by the spreading phase of the water droplet. Similarly, the droplet has a thickness (lamella) of 2.45 mm, Fig. 5 (b), at the initial stage due to the spherical nature of the drop. As it deforms to reach a maximum spreading, the thickness of the droplet is 0.71 mm at 3.4 ms before it starts to recoil.

When a triangular-like relief with surface fraction ($\phi_s$) of 0.375 $\mu m^2$ was introduced on Ti-6Al-4V surface, as presented in Fig. 4(a), the evolution of the water droplet and wettability changes significantly (Fig. 6(b)) . In fact, when the droplet start to spread at 8 $\mu s$, an air bubble was observed at the centre of the droplet, which is not only due to capillary force alone [31] but also depends on the introduced roughness. The $\phi_s$ of solid Ti-6Al-4V surface covered by the water droplet is zero as it is assumed to be smooth and the calculated $\theta_{ECA}$ at maximum spreading diameter is $102^o$, Fig. 7(bI). However, when triangular relief was
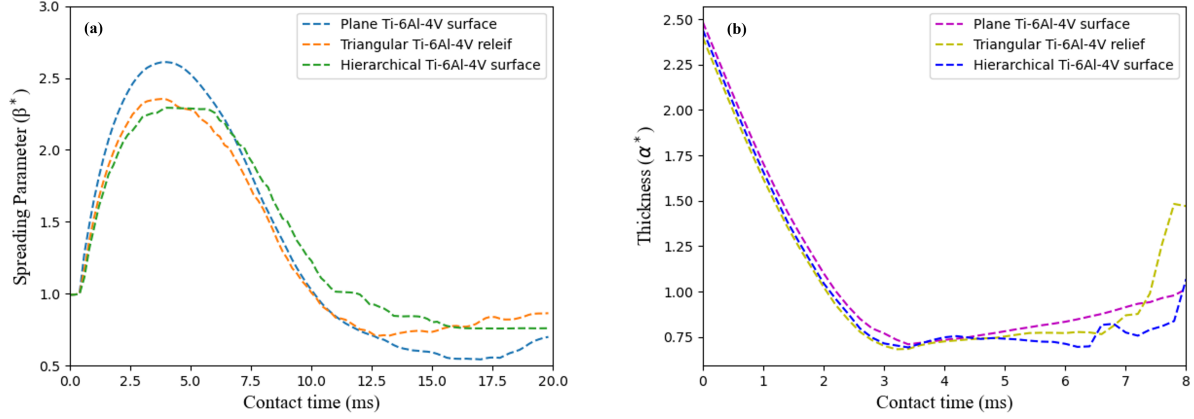
Figure 5: (a) Spreading parameter ($\beta^*$) and (b) thickness ($\alpha^*$) of water droplet on plain, triangular and hierarchical Ti-6Al-4V alloy surface.

introduced, it reaches the maximum spreading diameter at 3.8ms with $\phi_s$ of 9.9 $\mu m^2$ at an increased $\theta_{ECA}$ of $120^o$ (Fig. 7(bII)) contrary to that on the smooth surface. In addition, when the height (p) of the triangular relief was increased (in-between two triangles) as shown in Fig.4b to create a hierarchical surface, the maximum spreading diameter observed is 2.25mm. Here, $\phi_s$ covered by water is 10.7 $\mu m^2$ at the calculated $\theta_{ECA}$ of $122^o$ as presented in Fig. 7(bIII). The hydrodynamic trend is similar to that of plain Ti-6Al-4V as shown in Fig. 6 (a) and (c). The $\phi_s$ for the two introduced reliefs shows that the spreading parameter becomes weaker as the roughness scale increases, Fig. 5(a). Nonetheless, the reliefs still favor a rim-like structure formation at the periphery of the droplet with an increase in contact angle of the droplet. The effect of the roughness scale impact on the spreading diameter of water droplet corresponds to the one in the study of Chamakos et. al. [23]. Though, Chamakos et. al. [23] used a high viscous fluid, our results with with the increased viscosity are still in close agreement (see Fig. 8 (d) - (f) in section 3.3). Interestingly, the surface roughness holds the droplet in the area of maximum spread, with triangular relief primarily being in Wenzel-Cassie state and the hierarchical relief being in Wenzel state. The calculated $\theta_{ECA}$ at maximum $\beta^*$ for the three surfaces as shown in Fig. 7 (bI, bII and bIII) are $102^o$, $120^o$ and $122^o$ respectively. The measured measured $\theta_{ECA}$ is used in the next section to validate the maximum spreading diameter based on energy analysis. It should be noted that the $\theta_{ECA}$ for maximum $\theta_{ECA}$ was calculated by using the open source software [34].

## 3.2. Effects of surface reliefs on maximum spreading based on energy analysis of droplet on several textured Ti-6Al-4V surfaces

We further compared the results of the maximum spreading diameter ($\beta^*$) of water droplet on the three surfaces with already established analytical models available in the literature and based on Re, We and $\theta_{ECA}$. Such scaling parameters and several scaling laws were extensively used to predict the maximum spreading diameter of liquid droplets on solid surfaces [29]. The applicability, consistency and reliability to capture droplet impact process of such laws are, however, very questionable [29]. Here we only used these parameters to simplify the analysis,
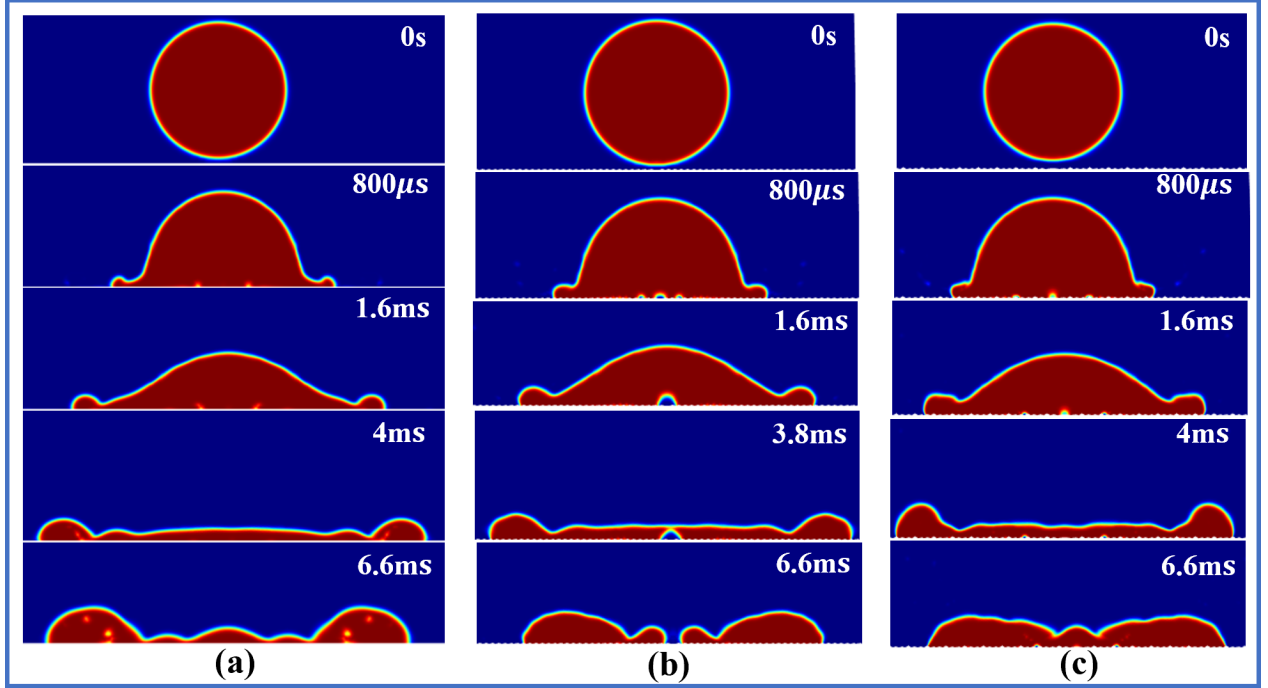
Figure 6: Snapshot of water impact on (a) solid, (b) triangular, and (c) hierarchical Ti-6Al-4V alloy surface with $u_o$ of 1m/s at $\theta_{ECA}$ of $96^o$.

but not the laws themselves. In fact, because our model describes the droplet dynamics, we can also use it to verify the validity of these descriptions.

$$\beta_{max} = \frac{d_{max}}{D_o} = \sqrt{\frac{We + 12}{3(1 - cos(\theta_{ECA})) + 4(We/\sqrt{Re})}} \tag{10}$$

For this purpose, a simplified energy conservation model for a droplet on solid surfaces can be used. Among the available models, the analytical model of Pasandideh-Fard et. al. [35], which predicts the maximum $\beta^*$ after droplet impact based on energy conservation looks particularly interesting. This model uses the kinetic energy, surface energy and viscous dissipation before and after impact. The solid surface energy is assumed to be zero, that is, the total surface energy consists of only the liquid-vapor surface energy which is the product of the droplet surface area and the liquid-vapor surface tension [32][36]. The results of our numerical calculation and that of the analytical model for maximum $\beta^*$ of water droplet on plan Ti-6Al-4V and surfaces with triangular and hierarchical reliefs based on previously stated values of Re and We are summarised in Table 2. The maximum spreading diameter for solid Ti-6Al-4V surface of our calculation is in a good agreement with that of [35]. It is also interesting that the model can predict maximum $\beta^*$ on both triangular and hierarchical Ti-6Al-4V surface reliefs. While the Pasandideh-Fard [35] model overestimates the maximum $\beta^*$ measured in experiment by 15%, our numerical results deviate by 9.7% from the results of this model. Fig. 7(a) shows such deviation in $\beta^*$ and $\theta_{ECA}$ of the three surfaces. Additionally, Fig. 7 (bI, bII and bIII) shows the $\theta_{ECA}$ used in the calculations, and the fraction area ($\phi_s$) of the structure covered by water.
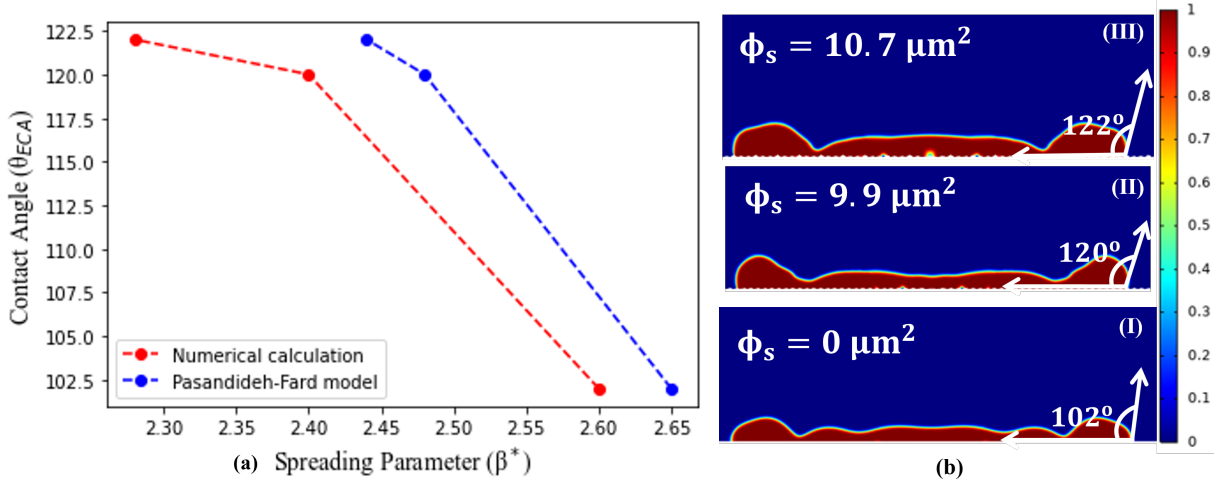
Figure 7: (a) Comparison of spreading parameter ($\beta^*$) of the current study with [35] and (b) measured equilibrium contact $\theta_{ECA}$ with area fraction ($\phi_s$) covered by water on (I) plain, (II) triangular and (III) hierarchical surface reliefs.

Table 2: Maximum $\beta^*$ of the current study and that of the analytical solution

| Surfaces | Max. $\beta^*$ (current study) | Analytical solution [35] |
|---|---|---|
| Plain Ti-6Al-4V | 2.60 | 2.65 |
| Triangular Ti-6Al-4V | 2.40 | 2.48 |
| Hierarchical Ti-6Al-4V | 2.28 | 2.44 |

### 3.3. Effect of velocity and viscosity of droplet on femtosecond textured Ti-6Al-4V relief surfaces

By varying the initial impact velocity ($u_o$) from 0.8m/s to 1.1m/s and the viscosity of droplet from 1 $\mu m$ to 31 $\mu m$ on solid, triangular and hierarchical Ti-6Al-4V surface, the evolution of the spreading parameter with the contact time are illustrated in Fig. 8 (a) - (f) respectively. For the simulation results shown in Fig. 8 (a) - (c), a dynamic viscosity of 1 mPas is set and the corresponding We ranges from 21 to 39, while Re is 1876 to 2580. In addition, the velocity of 1 m/s is maintained for Fig. 8 (d) - (f) and the We of 32 and Re ranges from 2345 to 77. The spreading parameter $\beta^*$ increases as the velocity rises for the three surfaces as presented in Fig 8(a) to (c). Interestingly, the contact time for the impact velocities, for which the droplet reaches a maximum $\beta^*$, is larger for a plain Ti-6Al-4V surface before the droplet starts to rapidly recoil on the surface. For triangular and hierarchical reliefs, the contact time is lower for the droplet to reach a maximum $\beta^*$ and this is due to the roughness scale. Though even when the velocity increases on the relief surfaces, droplet does not rapidly spread on the surfaces compared to that of plain Ti-6Al-4V surface. However, as the viscosity of the droplet becomes larger, the impact process of the droplet on the surfaces is slowed down due to the viscous dissipation. As a result, the spreading parameter decreases as presented in Fig. 8 (d) to (f). The contact time, for which the droplet reaches a maximum $\beta^*$, becomes smaller on the triangular and hierarchical reliefs as
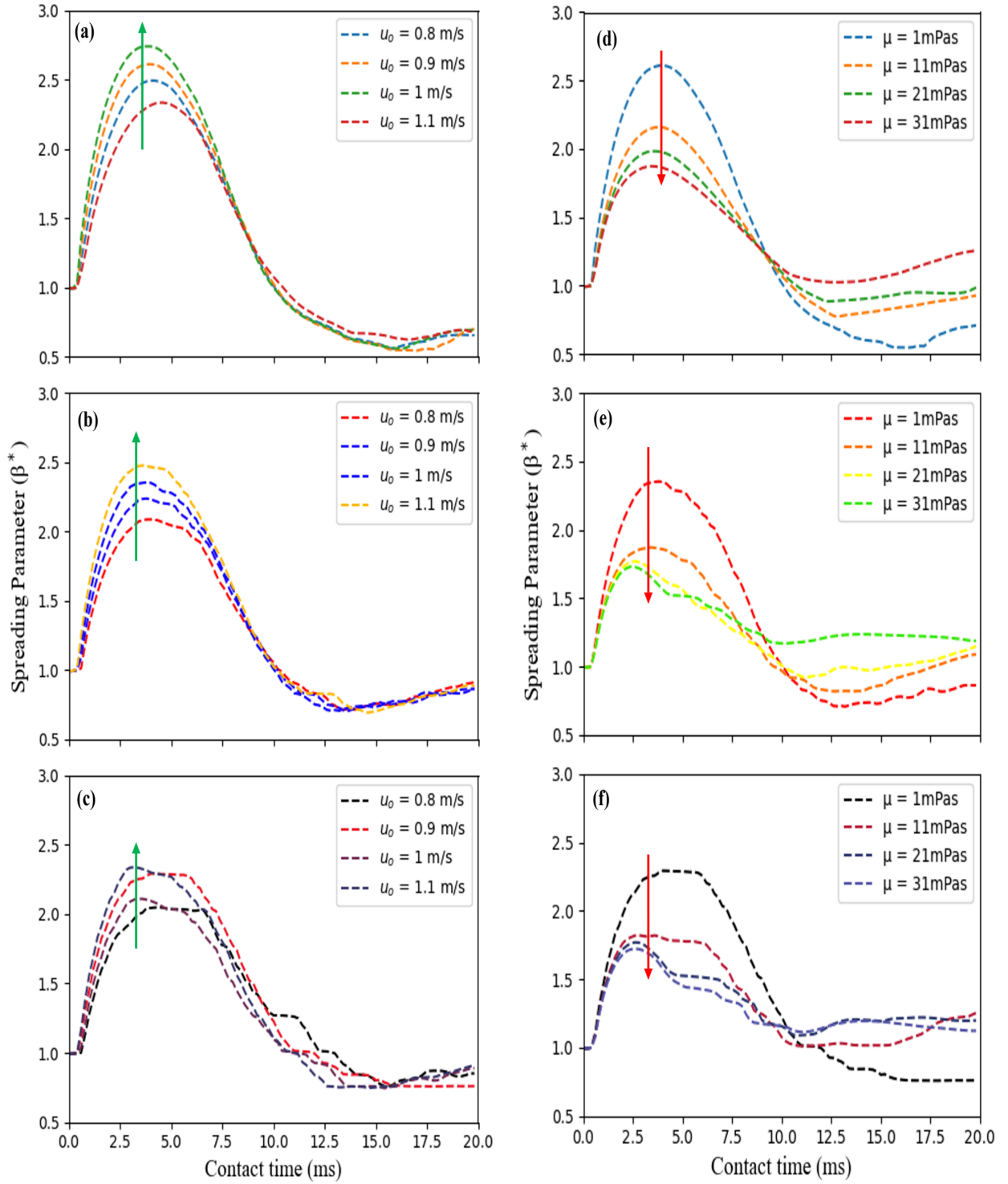
Figure 8: Spreading parameter ($\beta^*$) at $u_o = 0.8$m/s - 1.1m/s (a) - (f) and $\mu = 1$ mPas - 31 mPs for plan, triangular and hierarchical Ti-6Al-4V alloy surface.

a result of the roughness.

### 3.4. Conclusion

In this study, numerical studies of the effect of surface reliefs, impact velocity, viscosity on wettability and droplet dynamics on Ti-6Al-4V surfaces was examined. The main conclusions of this study are summarise as follows:

(i) Firstly, on plain Ti-6Al-4V surface, the droplet spreads rapidly due to the interplay between the inertial and capillary forces upon the impact with increased spreading parameter. The droplet rapidly rebounds afterwards due to the capillary force. For higher viscosity, the spreading process slows down with a decrease in the spreading parameter. The maximum spreading diameter of the droplet of the current study is in close agreement with the analytical model of Pasandideh-Fard [35] that is based on the energy balance for a liquid droplet on different surfaces.

(ii) When surface reliefs were introduced, the spreading parameter were weaker, but favored wettability as the contact angle at the periphery increases. This results is due to the change in roughness scale from triangular to hierarchical reliefs. With this, the surface roughness is shown to hold the droplet. In fact, air bubbled is entrapped at the initial stage and the triangular relief can be considered to be in the Wenzel-Cassie state, while the hierarchical relief, is in the Wenzel state. As impact velocity on these reliefs increases, the spreading diameter of the droplet rises up. The time it takes to reach the maximum spreading is, however, shorter than that on the plane Ti-6Al-4V surface. At low viscosity, the spreading parameter is high, but as the viscosity increases, the droplet diameter significantly decays. On the textured surfaces this is due to the roughness.

Therefore, we conclude that surface reliefs play a crucial role in spreading behavior of the liquid droplet and that hierachical reliefs are promising for the wettability enhancement. In addition, spreading increases with impact velocity and decreases with liquid velocity on both plain and surfaces with different reliefs.

**Note:.** The authors declare no conflicts of interest.

### References

[1] J. Bonse, J. Krüger, S. Höhm, A. Rosenfeld, Femtosecond laser-induced periodic surface structures, Journal of Laser Applications 24 (2012) 042006. URL: https://doi.org/10.2351/1.4712658. doi:10.2351/1.4712658. arXiv:https://doi.org/10.2351/1.4712658.

[2] A.-M. Kietzig, S. G. Hatzikiriakos, P. Englezos, Patterned superhydrophobic metallic surfaces, Langmuir 25 (2009) 4821–4827. URL: https://doi.org/10.1021/la8037582. doi:10.1021/la8037582. arXiv:https://doi.org/10.1021/la8037582, pMID: 19267439.

[3] P. Bizi-bandoki, S. Valette, E. Audouard, S. Benayoun, Time dependency of the hydrophilicity and hydrophobicity of metallic alloys subjected to femtosecond laser irradiations, Applied Surface Science 273 (2013) 399–407. URL: https://www.sciencedirect.com/science/article/pii/S0169433213003620. doi:https://doi.org/10.1016/j.apsusc.2013.02.054.

[4] N. B. Dahotre, S. R. Paital, A. N. Samant, C. Daniel, Wetting behaviour of laser synthetic surface microtextures on ti&#x2013;6al&#x2013;4v for bioapplication, Philosophical Transactions of the Royal Society A: Mathematical, Physical and Engineering Sciences 368 (2010) 1863–1889. URL: https://royalsocietypublishing.org/doi/abs/10.1098/rsta.2010.0003. doi:10.1098/rsta.2010.0003.

[5] X. Liu, P. K. Chu, C. Ding, Surface modification of titanium, titanium alloys, and related materials for biomedical applications, Materials Science and Engineering: R: Reports 47 (2004) 49–121. URL: `https://www.sciencedirect.com/science/article/pii/S0927796X0400124X`. doi:`https://doi.org/10.1016/j.mser.2004.11.001`.

[6] W. Barthlott, C. Neinhuis, Purity of the sacred lotus, or escape from contamination in biological surfaces, Planta 202 (1997) 1–8. URL: `https://doi.org/10.1007/s004250050096`. doi:`10.1007/s004250050096`.

[7] A. Y. Vorobyev, C. Guo, Direct femtosecond laser surface nano/microstructuring and its applications, Laser & Photonics Reviews 7 (2013) 385–407. doi:`https://doi.org/10.1002/lpor.201200017`.

[8] J. Yong, F. Chen, Q. Yang, Z. Jiang, X. Hou, A review of femtosecond-laser-induced underwater superoleophobic surfaces, Advanced Materials Interfaces 5 (2018) 1701370. URL: `https://onlinelibrary.wiley.com/doi/abs/10.1002/admi.201701370`. doi:`https://doi.org/10.1002/admi.201701370`.

[9] A. Cunha, A. P. Serro, V. Oliveira, A. Almeida, R. Vilar, M.-C. Durrieu, Wetting behaviour of femtosecond laser textured ti-6al-4v surfaces, Applied Surface Science 265 (2013) 688–696. URL: `https://www.sciencedirect.com/science/article/pii/S0169433212020430`. doi:`https://doi.org/10.1016/j.apsusc.2012.11.085`.

[10] A. Klos, X. Sedao, T. E. Itina, C. Helfenstein-Didier, C. Donnet, S. Peyroche, L. Vico, A. Guignandon, V. Dumas, Ultrafast laser processing of nanostructured patterns for the control of cell adhesion and migration on titanium alloy, Nanomaterials 10 (2020). URL: `https://www.mdpi.com/2079-4991/10/5/864`. doi:`10.3390/nano10050864`.

[11] T. Young, An essay on the cohesion of fluids, Abstracts of the Papers Printed in the Philosophical Transactions of the Royal Society of London 1 (1832) 171–172. URL: `https://royalsocietypublishing.org/doi/abs/10.1098/rspl.1800.0095`. doi:`10.1098/rspl.1800.0095`.

[12] R. N. Wenzel, Surface roughness and contact angle., The Journal of Physical and Colloid Chemistry 53 (1949) 1466–1467. URL: `https://doi.org/10.1021/j150474a015`. doi:`10.1021/j150474a015`. arXiv:`https://doi.org/10.1021/j150474a015`.

[13] R. N. Wenzel, Resistance of solid surfaces to wetting by water, Industrial & Engineering Chemistry 28 (1936) 988–994. URL: `https://doi.org/10.1021/ie50320a024`.

[14] A. B. D. Cassie, S. Baxter, Wettability of porous surfaces, Trans. Faraday Soc. 40 (1944) 546–551. URL: `http://dx.doi.org/10.1039/TF9444000546`. doi:`10.1039/TF9444000546`.

[15] T. Onda, S. Shibuichi, N. Satoh, K. Tsujii, Super-water-repellent fractal surfaces, Langmuir 12 (1996) 2125–2127. URL: `https://doi.org/10.1021/la950418o`. doi:`10.1021/la950418o`. arXiv:`https://doi.org/10.1021/la950418o`.

[16] S. Shibuichi, T. Onda, N. Satoh, K. Tsujii, Super water-repellent surfaces resulting from fractal structure, The Journal of Physical Chemistry 100 (1996) 19512–19517. URL: `https://doi.org/10.1021/jp9616728`. doi:`10.1021/jp9616728`. arXiv:`https://doi.org/10.1021/jp9616728`.

[17] J. Drelich, E. Chibowski, Superhydrophilic and superwetting surfaces: Definition and mechanisms of control, Langmuir 26 (2010) 18621–18623. URL: `https://doi.org/10.1021/la1039893`. doi:`10.1021/la1039893`. arXiv:`https://doi.org/10.1021/la1039893`, pMID: 21090661.

[18] D. Quéré, Non-sticking drops 68 (2005) 2495–2532. URL: `https://doi.org/10.1088/0034-4885/68/11/r01`. doi:`10.1088/0034-4885/68/11/r01`.

[19] J. B. Bico, U. Thiele, D. Quéré, Wetting of textured surfaces, Colloids and Surfaces A: Physicochemical and Engineering Aspects 206 (2002) 41–46. URL: `https://www.sciencedirect.com/science/article/pii/S0927775702000614`. doi:`https://doi.org/10.1016/S0927-7757(02)00061-4`.

[20] G. McHale, Cassie and wenzel:â€‰ were they really so wrong?, Langmuir 23 (2007) 8200–8205. URL: `https://doi.org/10.1021/la7011167`. doi:`10.1021/la7011167`. arXiv:`https://doi.org/10.1021/la7011167`, pMID: 17580921.

[21] S. Sikalo, H.-D. Wilhelm, I. V. Roisman, S. Jakirlić, C. Tropea, Dynamic contact angle of spreading droplets: Experiments and simulations, Physics of Fluids 17 (2005) 062103. URL: `https://doi.org/10.1063/1.1928828`. doi:`10.1063/1.1928828`. arXiv:`https://doi.org/10.1063/1.1928828`.

[22] H. Grewal, I.-J. Cho, J.-E. Oh, E.-S. Yoon, Effect of topography on the wetting of nanoscale patterns: experimental and modeling studies, Nanoscale 6 (2014) 15321–15332. URL: `http://dx.doi.org/10.1039/C4NR04069D`. doi:`10.1039/C4NR04069D`.

[23] N. T. Chamakos, M. E. Kavousanakis, A. G. Boudouvis, A. G. Papathanasiou, Droplet spreading on rough surfaces: Tackling the contact line boundary condition, Physics of Fluids 28 (2016) 022105. URL: `https://doi.org/10.1063/1.4941577`. doi:`10.1063/1.4941577`. arXiv:`https://doi.org/10.1063/1.4941577`.

[24] A. Yagub, H. Farhat, S. Kondaraju, T. Singh, A lattice boltzmann model for substrates with regularly structured surface roughness, Journal of Computational Physics 301 (2015) 402–414. URL: `https://www.sciencedirect.com/science/article/pii/S0021999115005689`. doi:`https://doi.org/10.1016/j.jcp.2015.08.040`.

[25] X. Shan, H. Chen, Lattice boltzmann model for simulating flows with multiple phases and components, Phys. Rev. E 47 (1993) 1815–1819. URL: `https://link.aps.org/doi/10.1103/PhysRevE.47.1815`. doi:`10.1103/PhysRevE.47.1815`.

[26] E. Olsson, G. Kreiss, A conservative level set method for two phase flow, Journal of Computational Physics 210 (2005) 225–246. URL: `https://www.sciencedirect.com/science/article/pii/S0021999105002184`. doi:`https://doi.org/10.1016/j.jcp.2005.04.007`.

[27] COMSOL, Comsol multiphysics (2021) 1742.

[28] R. Tadmor, Line energy and the relation between advancing, receding, and young contact angles, Langmuir 20 (2004) 7659–7664. URL: `https://doi.org/10.1021/la049410h`. doi:`10.1021/la049410h`. arXiv:`https://doi.org/10.1021/la049410h`, pMID: 15323516.

[29] S. Lin, B. Zhao, S. Zou, J. Guo, Z. Wei, L. Chen, Impact of viscous droplets on different wettable surfaces: Impact phenomena, the maximum spreading factor, spreading time and post-impact oscillation, Journal of Colloid and Interface Science 516 (2018) 86–97. URL: `https://www.sciencedirect.com/science/article/pii/S0021979717314765`. doi:`https://doi.org/10.1016/j.jcis.2017.12.086`.

[30] K. Yokoi, D. Vadillo, J. Hinch, I. Hutchings, Numerical studies of the influence of the dynamic contact angle on a droplet impacting on a dry surface, Physics of Fluids 21 (2009) 072102. URL: `https://doi.org/10.1063/1.3158468`. doi:`10.1063/1.3158468`. arXiv:`https://doi.org/10.1063/1.3158468`.

[31] V. Mehdi-Nejad, J. Mostaghimi, S. Chandra, Air bubble entrapment under an impacting droplet, Physics of Fluids 15 (2003) 173–183. URL: `https://doi.org/10.1063/1.1527044`. doi:`10.1063/1.1527044`. arXiv:`https://doi.org/10.1063/1.1527044`.

[32] T. Mao, D. C. S. Kuhn, H. Tran, Spread and rebound of liquid droplets upon impact on flat surfaces, AIChE Journal 43 (1997) 2169–2179. URL: `https://aiche.onlinelibrary.wiley.com/doi/abs/10.1002/aic.690430903`. doi:`https://doi.org/10.1002/aic.690430903`.

[33] R. Fang, Z. Li, X. Zhang, X. Zhu, H. Zhang, J. Li, Z. Pan, Z. Huang, C. Yang, J. Zheng, W. Yan, Y. Huang, V. S. Maisotsenko, A. Y. Vorobyev, Spreading and drying dynamics of water drop on hot surface of superwicking ti-6al-4v alloy material fabricated by femtosecond laser, Nanomaterials 11 (2021). URL: `https://www.mdpi.com/2079-4991/11/4/899`. doi:`10.3390/nano11040899`.

[34] C. A. Schneider, W. S. Rasband, K. W. Eliceiri, Nih image to imagej: 25 years of image analysis, Nature Methods 9 (2012) 671–675. URL: `https://doi.org/10.1038/nmeth.2089`. doi:`10.1038/nmeth.2089`.

[35] M. Pasandideh-Fard, Y. M. Qiao, S. Chandra, J. Mostaghimi, Capillary effects during droplet impact on a solid surface, Physics of Fluids 8 (1996) 650–659. URL: `https://doi.org/10.1063/1.868850`. doi:`10.1063/1.868850`.

[36] H.-M. Huang, X.-P. Chen, Energetic analysis of drop's maximum spreading on solid surface with low impact speed, Physics of Fluids 30 (2018) 022106. URL: `https://doi.org/10.1063/1.5006439`. doi:`10.1063/1.5006439`.